ADVANCED MATERIALS
www.advmat.de

Piezophototronic Effect in Single-Atomic-Layer MoS_2 for Strain-Gated Flexible Optoelectronics

*Wenzhuo Wu, Lei Wang, Ruomeng Yu, Yuanyue Liu, Su-Huai Wei, James Hone, and Zhong Lin Wang**

Dynamic manipulation of electronic and optical processes in optoelectronics is usually achieved by applying an electrostatic bias.[1,2] However, emerging applications in wearable devices and human–machine interfacing desire that functional optoelectronics can be directly regulated by mechanical stimuli/inputs from human body.[3–5] Here, we report strain-gated flexible optoelectronics based on monolayer piezoelectric-semiconductor MoS_2. Utilizing the piezoelectric polarization charges created at the metal–MoS_2 interface to modulate the separation/transport of photogenerated carriers, the piezophototronic effect is applied to implement two-terminal atomic-layer-thick phototransistor, in which the photodetection is systematically tuned by substrate-induced strain. A maximum photoresponsivity of 2.3×10^4 A W^{-1} with a 26-fold improvement over the reported highest photoresponsivity for monolayer MoS_2 phototransistors is demonstrated when a –0.38% compressive static strain is introduced at low illumination intensity of 3.4 μW cm^{-2} (wavelength = 442 nm). The coupling among piezoelectricity, optical excitation, and semiconducting properties in 2D atomically thin materials may enable the development of flexible nanooptoelectromechanical systems, adaptive bioopto-electronic probes, and ultrathin optoelectronics.

The seamless and adaptive interactions between micro/nano-systems and physical environment are crucial for advancing wearable technology, healthcare, robotics, distributed sensing, and advanced manufacturing,[3,6] which demand the detection, processing and control of information encoded in environmental stimuli by functional devices. Non-electrical stimuli, e.g., mechanical agitations, are ubiquitous and abundant in the environment for powering and controlling the micro/nano-devices.[4,5] Nevertheless, it is not facile to directly interface mechanical stimuli using the state-of-the-art technology that relies on electrical modulation of charge carriers in semiconductors. The piezoelectric effect, which produces polarization under mechanical deformation in materials lacking inversion symmetry or having polarization domains, has been intensively studied in bulk crystals, thin films, and nanostructures for electromechanical applications.[4,5,7] Recently, studies on the fundamental coupling between piezoelectric polarization, photon excitation and charge carrier processes under dynamic mechanical perturbation in wurtzite-structured semiconductors, e.g., ZnO and GaN, result in an emerging field of piezophototronics,[8,9] which has immediate relevance to the abovementioned applications. When a static strain is induced in a piezoelectric semiconductor, the presence of the localized polarization charges can effectively modulate/control the generation, separation, transport, and recombination of photoinduced charge carriers at the vicinity of a Schottky barrier or p-n junction, by exerting substantial influences on the concentration/distribution of free carriers and/or the modulation of electronic charge in interface states. This is the piezophototronic effect.[10] Devices using the piezoelectric polarization charges as a "gate" controlling signal to achieve tunable optoelectronic processes is piezophototronics.

With their outstanding semiconductor properties (e.g., bandgap ≈1–2 eV favorable for electronics and optoelectronics, room temperature mobility > 200 cm^2 V^{-1} s^{-1}, etc.),[11,12] superior optoelectronic performance (e.g., direct bandgap, high external photoresponsivity ≈880 A W^{-1}, valley polarization longer than 1 ns, etc.),[12,13] and the ability to withstand enormous strain (e.g., monolayer MoS_2 crystal can be deformed by 11% strain without fracture),[14] 2D transition metal dichalcogenides (TMDCs) are of great interest as building blocks for mechanically compliant optoelectronics. Moreover, monolayer TMDCs become noncentrosymmetric and exhibit piezoelectricity.[15,16] Here, we report the first experimental observation of piezophototronic effect in single-atomic-layer 2D MoS_2 and its application in strain-gated adaptive photodetection. The strain-induced polarization charges in single-layer MoS_2 can modulate the separation and transport of photogenerated carriers at the MoS_2–metal barrier and enable tunable photodetection, with a maximum photoresponsivity of 2.3×10^4 A W^{-1} under –0.38% compressive strain, which presents a 26-fold improvement over the highest photoresponsivity previously reported for monolayer MoS_2 phototransistors.[2] This is also the first demonstration of single-atomic-layer 2D TMDC based flexible optoelectronic devices.

Dr. W. Z. Wu, Dr. R. M. Yu, Prof. Z. L. Wang
School of Materials Science and Engineering
Georgia Institute of Technology
Atlanta, GA 30332-0245, USA
E-mail: zhong.wang@mse.gatech.edu
Dr. L. Wang
Department of Electrical Engineering
Columbia University
New York, NY 10027, USA
Dr. Y. Y. Liu, Dr. S.-H. Wei
National Renewable Energy Laboratory (NREL)
Golden, CO 80401, USA
Prof. J. Hone
Department of Mechanical Engineering
Columbia University
New York, NY 10027, USA
Prof. Z. L. Wang
Beijing Institute of Nanoenergy and Nanosystems
Chinese Academy of Sciences
100083 Beijing, China

DOI: 10.1002/adma.201602854

© 2016 WILEY-VCH Verlag GmbH & Co. KGaA, Weinheim

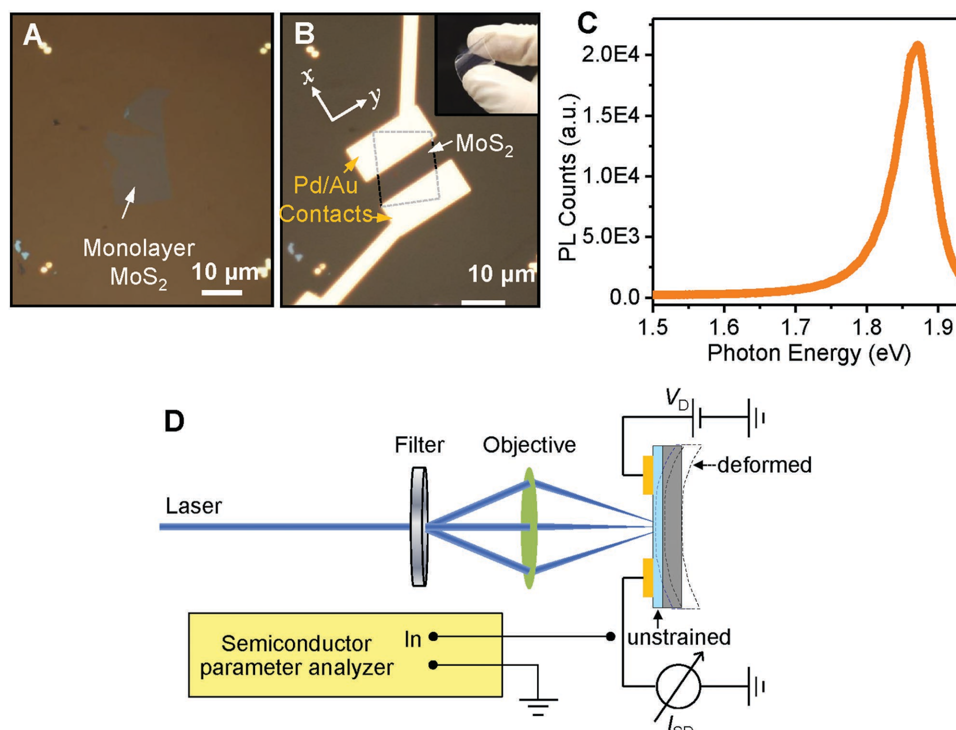

Figure 1. Single-layer MoS_2 piezophototronic device and operation scheme. a) Optical image of the single-atomic layer MoS_2 flake transferred onto PET flexible substrate. b) A flexible two-terminal single-atomic layer MoS_2 device. c) Typical PL spectrum of single-layer MoS_2 flakes. d) The home-customized setup for characterizing piezophototronic process in single-layer MoS_2.

In our experiments, single-layer MoS_2 flakes were prepared through mechanical exfoliation, and their crystallographic orientations that are important for piezophototronic applications were determined via second-harmonic generation using previously described methods.[15,17] Flakes were subsequently transferred onto a polyethylene terephthalate (PET) flexible substrate[18] (**Figure 1**a). Figure 1b shows a typical flexible two-terminal device with single-layer MoS_2 flake outlined by black dashed line. The lattice orientation of a single-layer MoS_2 is schematically depicted; the x-axis is taken to be along the "armchair" direction, and the y-axis along the "zigzag" direction. Electrical contacts made of Cr/Pd/Au (1 nm/20 nm/50 nm) were deposited with the metal–MoS_2 interface parallel to the y-axis. Photoluminescence (PL) measurement was performed using 633 nm laser excitation following previously reported methods.[12] The observed PL spectrum of single-layer MoS_2 flakes consists of a single narrow peak centered at 1.87 eV with 50 meV width, which is attributed to the direct-gap luminescence[12,19] (Figure 1c). We studied the piezophototronic process in single-layer MoS_2 using a home-made setup (Figure 1d and Methods section, Supporting Information), by measuring the photocurrent under systematically tuned optical illuminations and mechanical strains. A focused laser beam (wavelength 442 nm, ≈2 mm diameter) is illuminated over the device. When the substrate is mechanically bent, uniaxial strain is induced in MoS_2 with magnitude proportional to the curvature (Figure 1d, and Figure S1 and Note S1, Supporting Information). In our experiment, the applied strain is limited to 0.8% to avoid sample slippage.[15,20]

Figure 2a shows the photoresponse in single-layer device when there is no strain applied. A photoresponse from the same device when the drain bias extends to 2 V is included in Figure S2 (Supporting Information). The as-fabricated metal–semiconductor–metal (MSM) photodetector consists of two back-to-back Schottky barriers, and transport across the reversely biased Pd-MoS_2 Schottky barrier limits the current flow[15] (Note S2, Supporting Information). The I_{ds}–V_{ds} curves in Figure 2a and Figure S2 (Supporting Information) were measured in the dark and under different illumination intensities, with the polarity of the applied voltage defined with respect to the drain electrode. Strong rectification observed here indicates a significant asymmetry in the barrier characteristics, e.g., barrier heights, for the two Schottky contacts at drain and source electrodes, which may result from the difference in the effective areas and interface/surface states at the contacts.[5,9,10] The measured total current (I_{ds}) increases significantly from ≈90 nA in dark to ≈220 nA with 4.297 mW cm^{-2} illumination when a drain voltage of −2 V was applied (Figure 2a). The photocurrent I_{ph} ($I_{ph} = I_{light,total} - I_{dark}$) shows good linearity across a wide intensity range from µW cm^{-2} to mW cm^{-2} without saturation at high power levels (Figure 2a). In order to examine the response of the photocurrent to incident optical power, the photoresponsivity of the device is determined as $R = I_{ph}/P_i$, where P_i is the illumination power on the photodetector. At a low illumination intensity (3.4 µW cm^{-2}), the device reaches a photoresponsivity of 9084 A W^{-1}. The decrease in photoresponsivity at higher illumination intensities is due to trap states present inside MoS_2 or at the interface between MoS_2

© 2016 WILEY-VCH Verlag GmbH & Co. KGaA, Weinheim
Adv. Mater. 2016, DOI: 10.1002/adma.201602854

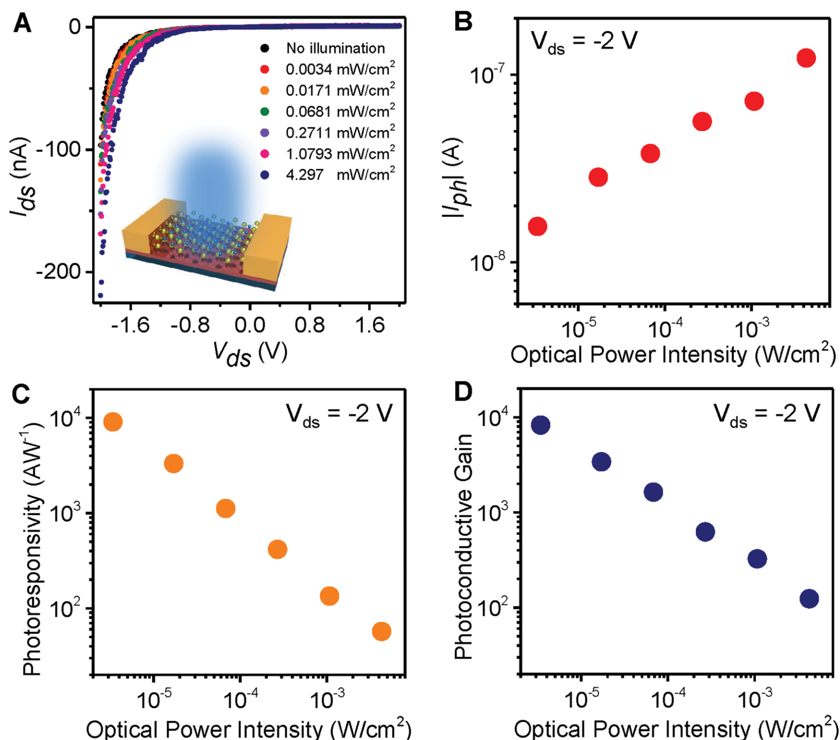

Figure 2. Photoresponse in single-layer MoS_2 photodetector when no strain is applied. a) Electrical transport in single-layer device in the dark and under different illumination intensities (wavelength = 442 nm). b–d) Photocurrent, photoresponsivity, and photoconductive gain of the single-layer device under –2 V drain bias.

and substrate.[2] The photoconductive gain (G), defined as the ratio between the number of electrons collected and the number of absorbed photons in the device per unit time, can be obtained using $G = (I_{ph}/P_i)/(h\nu/q)$, where h is Planck's constant, q is the electronic charge, and ν is the frequency of incident light. Figure 2D shows that G increases with decreasing excitation laser power and reaches ≈8260 when the excitation laser intensity is 3.4 µW cm^{-2}.

We next characterized the changes in photodetection properties of the devices with strain. The electrical transport under mechanical strain in a single-layer MoS_2 photodetector without optical illumination is shown in **Figure 3**a and Figure S3 (Supporting Information), presenting strong strain-dependence of the dark current. Mechanical strain can further modulate the photocurrent under different illumination intensities (Figure 3a). In our single-layer MoS_2 photodetector, changes in transport and photodetection behaviors with strain may arise from two effects: the piezophototronic effect,[10] in which strain-induced polarization charges at the Schottky barriers at the two ends of the MSM device may effectively separate the photogenerated carriers and control the transport of the charge carriers across the barriers; and the piezoresistive effect, where strain results in changes in band structure and density of states of the carriers.[21] To understand the underlying mechanism for the associated processes, the changes in dark current and photocurrent with strain under fixed drain bias (–2 V) are plotted in Figure 3b. When there is no light illumination, dark current in the single-layer device decreases with increasing compressive strain and increases with increasing tensile strain (Figure 3b, top). This asymmetric modulation is similar to the piezotronic effect reported for wurtzite-structured piezoelectric semiconductors, in which the piezoelectric polarization in the crystal can effectively tune the Schottky contact properties (Note S3 and Figure S4, Supporting Information). When laser illumination is on (Figure 3b, middle and bottom), the photocurrent decreases with increasing the tensile strain. Whereas, when compressive strain is applied, photocurrent first increases and then decreases with further increasing the magnitude of compressive strain. The device reaches the optimized photodetection under different compressive strains for low and high illumination intensities. At low illumination intensity (3.4 µW cm^{-2}), the device reaches a maximum photocurrent of 40 nA under –0.38% static strain; while at high illumination intensity (4.29 mW cm^{-2}), the maximum photocurrent (207 nA) occurs under a larger compressive strain (–0.45%). The strain dependence of photocurrent under various illumination intensities is obtained and shown in Figure S6 (Supporting Information). It can be seen that for all the illumination intensities, the photodetector has the smallest photocurrent when 0.62% strain is applied, compared to other strain conditions. The photodetector has the largest photocurrent when –0.38% strain is applied. The detailed explanation for this will be discussed later (in **Figure 4**). Moreover, the modulation effect of strain on the photocurrent is more significant when the illumination intensity is small (toward the left side of Figure S6, top panel, Supporting Information), while the corresponding modulation is less effective when the illumination intensity increases (toward the right side of Figure S6, top panel, Supporting Information). This suggests that the modulation effect of mechanical strain on photocurrent is also affected by the optical power intensity. The parameter $S = (I_{strain} - I_0)/I_0$, defined as the relative change in photocurrent by strain under certain illumination intensity, is plotted to quantitatively study this process (Figure 3c). Here I_{strain} and I_0 are the equilibrium photocurrent in the device with and without strain. It can be seen that values of S, which indicate the effectiveness of strain on modulating the photocurrent, decrease with increasing illumination intensity. This suggests that the gating effect of strain-induced polarization on photogenerated carriers is more significant at low optical illumination, which can be understood by taking into account the screening of piezoelectric polarization charges due to finite carrier density in monolayer MoS_2 at low light intensity.[15] At higher optical illumination, such screening is more significant due to increased free carrier density, and therefore the modulation of photocurrent by strain is less effective as compared to the case at low illumination intensity. Consequently, the compressive strain required for achieving optimized performance of the photodetector (e.g.,

© 2016 WILEY-VCH Verlag GmbH & Co. KGaA, Weinheim

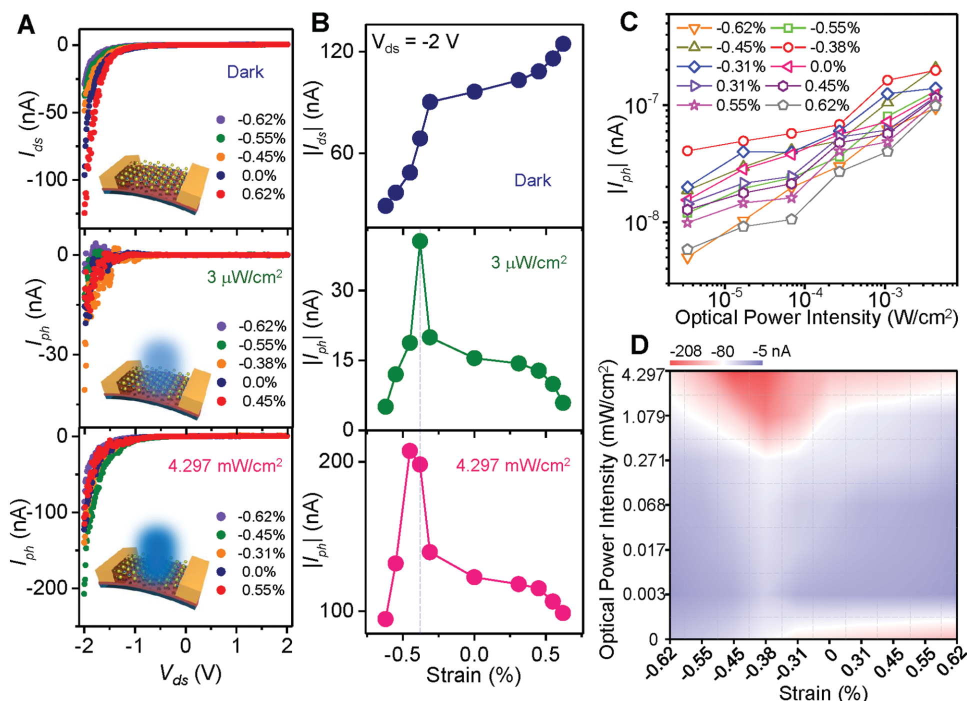

Figure 3. Piezophototronic response in single-layer MoS_2 photodetector. a) Top: Electrical transport in single-layer device in the dark under strains. Middle: Photocurrent in single-layer device under strains when the illumination intensity is low (3.4 μW cm^{-2}). Bottom: Photocurrent in single-layer device under strains when the illumination intensity is high (4.29 mW cm^{-2}). b) Strain dependence of the dark current (top) and photocurrent (middle and bottom) in single-layer device under −2 V drain bias. c) Relative change in photocurrent by strain (*S*) under different illumination intensities indicates the effectiveness of strain in modulating the photocurrent. d) A comprehensive piezophototronic mapping for photocurrent in single-layer device under different illumination intensities and mechanical strains. The drain bias is −2 V. The color gradient represents the photocurrent.

maximum I_{ph} and *S*) shifts to higher values when the illumination intensity increases (Figure 3c,d and Figure S6, Supporting Information).

The comprehensive mapping for photocurrent in single-layer device under different illumination intensities and mechanical strains has been plotted to provide insight in the underlying mechanism (Figure 3d). The dark current measured under different strains has also been included here. All of the I_{ph} curves (Figure 3d and Figure S6, Supporting Information) under different illumination intensities exhibit similar strain-dependence profile: they first increase to a maximum value when the applied compressive strain is small, and then decrease gradually when the compressive strain continues increasing. On the other hand, the I_{ph} always decreases with increasing the tensile strain. Moreover, the applied compressive strain corresponding to the maximum I_{ph} shifts to higher value when the illumination intensity increased. The contribution of piezoresistive effect that changes the electronic band structure has also been studied through first-principle calculation (Figure 5, Supporting Information). It can be seen that a tensile strain decreases the energies of both valence band maximum (VBM) and conduction band minimum (CBM) throughout the entire semiconductor, and therefore decreases the Schottky barrier height (SBH) for electrons and increases that for holes at both contacts. The effects are more prominent for CBM than VBM, hence the SBH for electrons are affected to a larger degree than holes. Thus one should expect an increase of the photocurrent at tensile strain because of the reduction of electron SBH, which disagrees with the experiments. Moreover, the simulation results show that piezoresistive effect can only result in a symmetric modulation in the device operation.

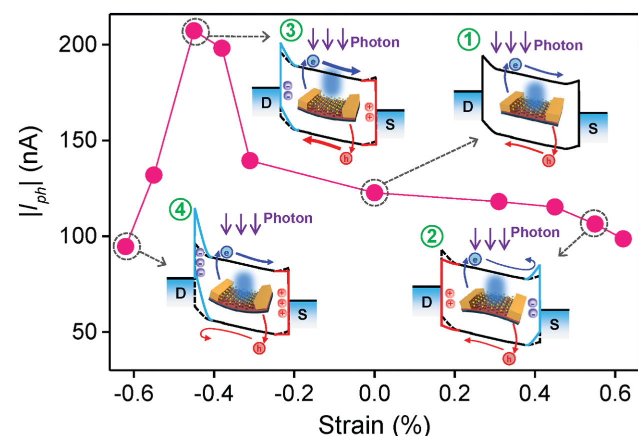

Figure 4. Working mechanism of piezophototronic response in single-layer MoS_2 photodetector. Band diagrams explaining the piezophototronic behavior observed in single-layer device as a result of the changes in Schottky barrier heights by strain-induced polarization (see text for details). The symbols "+" (in blue) and "–" (in red) represent the strain-induced positive and negative polarization charges.

To understand the observed phenomenon, the result obtained at a high illumination intensity (4.29 mW cm^{-2}) is used for describing the proposed mechanism (Figure 4). The

© 2016 WILEY-VCH Verlag GmbH & Co. KGaA, Weinheim
Adv. Mater. 2016, DOI: 10.1002/adma.201602854

incident photon induces electron–hole pairs in MoS_2. When there is no strain applied (1 in Figure 4), the electrons and holes are separated and collected by the built-in electric field at the Schottky contact and the applied external field. This gives rise to the photocurrent, which depends on the effective separation and transport of both holes and electrons at the vicinity of the contacts, and is strongly affected by the barrier characteristics. When a mechanical strain is applied to the device (2–4 in Figure 4), piezoelectric polarization charges induced at the zigzag edges can directly affect the metal–MoS_2 contacts, by modifying the concentration/distribution of free carriers in MoS_2 at the vicinity of the Schottky barrier,[10,15] such that the mechanical strain functions as a controlling gate signal to tune the optoelectronic processes, which is the piezophototronic effect. The distribution of piezoelectric polarization charges has been calculated previously using the density functional theory,[22] which also confirms the modulation effect of piezocharges on the metal–MoS_2 contacts. More detailed discussions on the modulation of Schottky barrier height by mechanical strain in various device structures that incorporate piezoelectric semiconductors can be found in previous reviews on piezotronics and piezophototronics,[10,23] as well as in reports studying the effect of depolarization field on the barrier by the associated interface dipole.[24] When a tensile strain is introduced (2 in Figure 4), due to the crystal orientation of the single-layer MoS_2, positive polarization charges are created at the reversely biased drain Schottky contact. The realigned band profile therefore provides a smaller driving force for the separation and redistribution of holes and electrons. Moreover, the energy barrier for electron transport at the positively biased contact is also increased. Therefore, the overall collection of photoinduced carriers in the device is suppressed. The carrier transport property is the result of the two processes depending on the magnitude of the applied strain. When a small compressive strain is applied (3 in Figure 4), low-density negative and positive polarization charges are created at the drain and source barriers; the resultant band tilting promotes the separation of holes and electrons in the active region, as well as their transport and collection at the contacts. Therefore, the observed photocurrent first increases with applied compressive strains. However, when a larger compression is induced beyond certain value, the up-bending of VBM is so significant that a new energy barrier arising from the local piezocharges for hole transport is introduced at the drain contact (4 in Figure 4). The holes would be trapped at the interface, which hinders the separation of photoexcited electron–hole pairs and promotes their recombination near the contact interface.[25] The related upward bending of the conduction band can lead to an increased dark current through enhanced tunneling events, which further deteriorates the overall photodetector performance. As a result, the photocurrent starts to decrease under large compressive strains. Such changes in band structure represent the formation of charge channels induced by the piezoelectric polarization in the depletion region of the Schottky contact. These charge channels can serve as effective means of modulating the carrier separation or recombination in the photodetector and other optoelectronic device. The existence of such charge channels has been validated by recent numerical calculations,[26] which clearly show that the formation of charge channel and related deformation of band profiles at the interface under strain can significantly affect the charge carrier transport, separation, and recombination processes. The theoretical support, in the forms of both analytical and numerical results, to the schematic band diagrams shown in Figure 4 can be found in previous theoretical studies.[26,27] The possible contribution of strain-gradient induced polarization on the observed device behavior due to flexoelectric effect may be safely ignored due to both the electrode configuration and the strain condition adopted in our experiment.[28] Nevertheless, the coupling between flexoelectricity and semiconductor properties in 2D materials is certainly an interesting avenue for future research.

Other figures of merit important to a photodetector, such as photoresponsivity, photoconductive gain, and sensitivity, can also be modulated and largely enhanced by mechanical strains (Figures 7–9, Supporting Information). These results suggest that mechanical strain is able to function as a controlling gate signal and effectively modulates the photodetection properties of single-layer MoS_2 optoelectronic device.

One other possible contribution to the photoresponse change in our devices could be strain-induced absorption change. However, first-principle calculations using density functional theory show that this effect is too small to account for the large photoresponse change (Methods section and Figure S10, Supporting Information). The absorption altered by a 0.6% tensile or compressive strain is insignificant compared with the experimentally observed change. In addition, our calculation suggests that a tensile strain increases the absorption, which is in contrast to the observed decrease in photocurrent. Therefore, the strain-induced absorption change cannot explain the experimental results. We conclude that piezophototronic effect due to the coupling among piezoelectricity, optical excitation, and semiconducting properties in single-layer MoS_2 gives rise to the observed photoresponse change by strain.

In summary, we have studied the piezophototronic effect in single-atomic-layer 2D MoS_2 and its application in strain-gated adaptive photodetection. Controllable modulation of M-S contacts or p-n junctions in 2D nanomaterials by strain-induced polarization may offer novel approach unavailable in conventional technologies using electrical control signals without modifying the interface structure/chemistry, for implementing tunable electronics and optoelectronics. Taking into account their superior mechanical properties, atomically thin 2D materials may excel other nanomaterials (e.g., nanowires) for piezophototronics applications, in terms of the life time and mechanical failure of the devices. However, 2D materials are more vulnerable to environmental conditions. For instance, their carrier concentrations may due to the environmental doping, which could result in variations in the screening process of piezocharges. By examining the crystal structure of a 2D material, it is anticipated that most 2D compounds in their monolayer form possess the noncentrosymmetric structure, and should be piezoelectric. It is expected that he strong coupling among piezoelectricity, optical excitation and semiconducting properties, together with the large mechanical stretchability/flexibility exhibited by single-atomic-layer compound materials may enable the development of flexible nanooptoelectromechanical systems, adaptive biooptoelectronic probes, and ultrathin optoelectronics.

© 2016 WILEY-VCH Verlag GmbH & Co. KGaA, Weinheim

Supporting Information

Supporting Information is available from the Wiley Online Library or from the author.

Acknowledgements

W.Z.W., L.W., and R.M.Y. contributed equally to this work. This research was supported by U.S. Department of Energy, Office of Basic Energy Sciences (Award DE-FG02-07ER46394), the National Science Foundation (DMR-1505319 and DMR-1122594). This work at NREL was supported by the U.S. Department of Energy under Contract No. DE-AC36-08GO28308. This work used the NREL Peregrine Supercomputer, and the National Energy Research Scientific Computing Center (NERSC), which is supported by the Office of Science of the U.S. Department of Energy under Contract No. DE-AC02-05CH11231. Z.L.W. acknowledges the "Thousands Talents" program for pioneer researcher and his innovation team, China and National Natural Science Foundation of China (Grant No. 51432005). W.Z.W. and Z.L.W. conceived the idea. W.Z.W., L.W., and Z.L.W. designed the experiments. L.W. and J.H. prepared the materials. L.W. and W.Z.W. fabricated the devices. W.Z.W., R.M.Y. and L.W. conducted the experiments. Y.Y.L. and S.H.W. performed the first-principle calculation. W.Z.W. and Z.L.W. analyzed the data and wrote the paper. All authors discussed the results and commented on the paper.

Received: May 30, 2016
Revised: July 7, 2016
Published online:

[1] a) Y. Cui, C. M. Lieber, *Science* **2001**, *291*, 851; b) B. W. H. Baugher, H. O. H. Churchill, Y. F. Yang, P. Jarillo-Herrero, *Nat. Nanotechnol.* **2014**, *9*, 262; c) J. S. Ross, P. Klement, A. M. Jones, N. J. Ghimire, J. Q. Yan, D. G. Mandrus, T. Taniguchi, K. Watanabe, K. Kitamura, W. Yao, D. H. Cobden, X. D. Xu, *Nat. Nanotechnol.* **2014**, *9*, 268; d) A. Pospischil, M. M. Furchi, T. Mueller, *Nat. Nanotechnol.* **2014**, *9*, 257.

[2] O. Lopez-Sanchez, D. Lembke, M. Kayci, A. Radenovic, A. Kis, *Nat. Nanotechnol.* **2013**, *8*, 497.

[3] a) D. H. Kim, R. Ghaffari, N. S. Lu, J. A. Rogers, *Annu. Rev. Biomed. Eng.* **2012**, *14*, 113; b) S. A. Morin, R. F. Shepherd, S. W. Kwok, A. A. Stokes, A. Nemiroski, G. M. Whitesides, *Science* **2012**, *337*, 828.

[4] Z. L. Wang, W. Z. Wu, *Angew. Chem., Int. Ed.* **2012**, *51*, 11700.

[5] W. Z. Wu, X. N. Wen, Z. L. Wang, *Science* **2013**, *340*, 952.

[6] J. R. Tumbleston, D. Shirvanyants, N. Ermoshkin, R. Janusziewicz, A. R. Johnson, D. Kelly, K. Chen, R. Pinschmidt, J. P. Rolland, A. Ermoshkin, E. T. Samulski, J. M. DeSimone, *Science* **2015**, *347*, 1349.

[7] A. I. Kingon, S. Srinivasan, *Nat. Mater.* **2005**, *4*, 233.

[8] a) Y. F. Hu, Y. Zhang, Y. L. Chang, R. L. Snyder, Z. L. Wang, *ACS Nano* **2010**, *4*, 4220; b) C. F. Pan, L. Dong, G. Zhu, S. M. Niu, R. M. Yu, Q. Yang, Y. Liu, Z. L. Wang, *Nat. Photonics* **2013**, *7*, 752; c) L. Dong, S. M. Niu, C. F. Pan, R. M. Yu, Y. Zhang, Z. L. Wang, *Adv. Mater.* **2012**, *24*, 5470; d) H. X. Li, Y. H. Yu, M. B. Starr, Z. D. Li, X. D. Wang, *J. Phys. Chem. Lett.* **2015**, *6*, 3410; e) S. Z. Yang, L. F. Wang, X. Z. Tian, Z. Xu, W. L. Wang, X. D. Bai, E. G. Wang, *Adv. Mater.* **2012**, *24*, 4676; f) M. B. Starr, J. Shi, X. D. Wang, *Angew. Chem. Int. Ed.* **2012**, *51*, 5962; g) J. Shi, P. Zhao, X. D. Wang, *Adv. Mater.* **2013**, *25*, 916; h) S. N. Lu, J. J. Qi, S. Liu, Z. Zhang, Z. Z. Wang, P. Lin, Q. L. Liao, Q. J. Liang, Y. Zhang, *ACS Appl. Mater. Inter.* **2014**, *6*, 14116; i) Y. Y. Chen, C. H. Wang, G. S. Chen, Y. C. Li, C. P. Liu, *Nano Energy* **2015**, *11*, 533; j) Y. Zhang, G. Y. Gao, H. L. W. Chan, J. Y. Dai, Y. Wang, J. H. Hao, *Adv. Mater.* **2012**, *24*, 1729.

[9] Q. Yang, Y. Liu, C. F. Pan, J. Chen, X. N. Wen, Z. L. Wang, *Nano Lett* **2013**, *13*, 607.

[10] Z. L. Wang, *Nano Today* **2010**, *5*, 540.

[11] a) Q. H. Wang, K. Kalantar-Zadeh, A. Kis, J. N. Coleman, M. S. Strano, *Nat. Nanotechnol.* **2012**, *7*, 699; b) B. Radisavljevic, A. Radenovic, J. Brivio, V. Giacometti, A. Kis, *Nat. Nanotechnol.* **2011**, *6*, 147.

[12] K. F. Mak, C. Lee, J. Hone, J. Shan, T. F. Heinz, *Phys. Rev. Lett.* **2010**, 105.

[13] a) F. H. L. Koppens, T. Mueller, P. Avouris, A. C. Ferrari, M. S. Vitiello, M. Polini, *Nat. Nanotechnol.* **2014**, *9*, 780; b) H. Zeng, J. Dai, W. Yao, D. Xiao, X. Cui, *Nat. Nanotechnol.* **2012**, *7*, 490.

[14] S. Bertolazzi, J. Brivio, A. Kis, *ACS Nano* **2011**, *5*, 9703.

[15] W. Z. Wu, L. Wang, Y. L. Li, F. Zhang, L. Lin, S. M. Niu, D. Chenet, X. Zhang, Y. F. Hao, T. F. Heinz, J. Hone, Z. L. Wang, *Nature* **2014**, *514*, 470.

[16] a) H. Y. Zhu, Y. Wang, J. Xiao, M. Liu, S. M. Xiong, Z. J. Wong, Z. L. Ye, Y. Ye, X. B. Yin, X. Zhang, *Nat. Nanotechnol.* **2015**, *10*, 151; b) K. A. N. Duerloo, M. T. Ong, E. J. Reed, *J. Phys. Chem. Lett.* **2012**, *3*, 2871; c) J. Qi, Y.-W. Lan, A. Z. Stieg, J.-H. Chen, Y.-L. Zhong, L.-J. Li, C.-D. Chen, Y. Zhang, K. L. Wang, *Nat. Commun.* **2015**, *6*, 7430; d) J. Zhang, C. Wang, C. Bowen, *Nanoscale* **2014**, *6*, 13314.

[17] Y. L. Li, Y. Rao, K. F. Mak, Y. M. You, S. Y. Wang, C. R. Dean, T. F. Heinz, *Nano Lett.* **2013**, *13*, 3329.

[18] C. R. Dean, A. F. Young, I. Meric, C. Lee, L. Wang, S. Sorgenfrei, K. Watanabe, T. Taniguchi, P. Kim, K. L. Shepard, J. Hone, *Nat. Nanotechnol.* **2010**, *5*, 722.

[19] A. Splendiani, L. Sun, Y. B. Zhang, T. S. Li, J. Kim, C. Y. Chim, G. Galli, F. Wang, *Nano Lett.* **2010**, *10*, 1271.

[20] C. R. Zhu, G. Wang, B. L. Liu, X. Marie, X. F. Qiao, X. Zhang, X. X. Wu, H. Fan, P. H. Tan, T. Amand, B. Urbaszek, *Phys. Rev. B* **2013**, *88*, 121301(R).

[21] Y. Y. Hui, X. F. Liu, W. J. Jie, N. Y. Chan, J. H. Hao, Y. T. Hsu, L. J. Li, W. L. Guo, S. P. Lau, *ACS Nano* **2013**, *7*, 7126.

[22] W. Liu, A. Zhang, Y. Zhang, Z. L. Wang, *App. Phy. Lett.* **2015**, *107*, 083105.

[23] a) Z. L. Wang, W. Z. Wu, *Natl. Sci. Rev.* **2014**, *1*, 62; b) Z. L. Wang, *Adv. Mater.* **2007**, *19*, 889; c) W. Wu, Z. L. Wang, *Nat. Rev. Mater.* **2016**, *1*(7), 16031.

[24] a) A. N. Morozovska, E. A. Eliseev, S. V. Svechnikov, A. D. Krutov, V. Y. Shur, A. Y. Borisevich, P. Maksymovych, S. V. Kalinin, *Phys. Rev. B.* **2010**, *81*, 205308; b) C. G. Duan, R. F. Sabirianov, W. N. Mei, S. S. Jaswal, E. Y. Tsymbal, *Nano Lett.* **2006**, *6*, 483; c) C. G. Duan, S. S. Jaswal, E. Y. Tsymbal, *Phy. Rev. Lett.* **2006**, *97*, 047201.

[25] P. Bhattacharya, *Semiconductor Optoelectronic Devices*, Prentice Hall, Upper Saddle River, NJ **1997**.

[26] Y. Liu, S. M. Niu, Q. Yang, B. D. B. Klein, Y. S. Zhou, Z. L. Wang, *Adv. Mater.* **2014**, *26*, 7209.

[27] a) Y. Zhang, Y. Liu, Z. L. Wang, *Adv. Mater.* **2011**, *23*, 3004; b) R. Araneo, F. Bini, M. Pea, A. Notargiacomo, A. Rinaldi, G. Lovat, S. Celozzi, *IEEE Trans. Nanotech.* **2014**, *13*, 724.

[28] a) P. V. Yudin, A. K. Tagantsev, *Nanotechnology* **2013**, *24* (43): 432001; b) P. Zubko, G. Catalan, A. K. Tagantsev, *Annu. Rev. Mater. Res* **2013**, *43*, 387; c) S. V. Kalinin, A. N. Morozovska, *Nat. Nanotechnol.* **2015**, *10*, 917.

© 2016 WILEY-VCH Verlag GmbH & Co. KGaA, Weinheim

DOI: 10.1002/adma.201602854